Logical computation demonstrated with a neutral atom quantum processor

Ben W. Reichardt,[1,3,*] Adam Paetznick,[1,*] David Aasen,[1] Ivan Basov,[1] Juan M. Bello-Rivas,[1] Parsa Bonderson,[1] Rui Chao,[1] Wim van Dam,[1] Matthew B. Hastings,[1] Andres Paz,[1] Marcus P. da Silva,[1] Aarthi Sundaram,[1] Krysta M. Svore,[1] Alexander Vaschillo,[1] Zhenghan Wang,[1] Matt Zanner,[1] William B. Cairncross,[2] Cheng-An Chen,[2] Daniel Crow,[2] Hyosub Kim,[2] Jonathan M. Kindem,[2] Jonathan King,[2] Michael McDonald,[2] Matthew A. Norcia,[2] Albert Ryou,[2] Mark Stone,[2] Laura Wadleigh,[2] Katrina Barnes,[2] Peter Battaglino,[2] Thomas C. Bohdanowicz,[2] Graham Booth,[2] Andrew Brown,[2] Mark O. Brown,[2] Kayleigh Cassella,[2] Robin Coxe,[2] Jeffrey M. Epstein,[2] Max Feldkamp,[2] Christopher Griger,[2] Eli Halperin,[2] Andre Heinz,[2] Frederic Hummel,[2] Matthew Jaffe,[2] Antonia M. W. Jones,[2] Eliot Kapit,[2,4] Krish Kotru,[2] Joseph Lauigan,[2] Ming Li,[2] Jan Marjanovic,[2] Eli Megidish,[2] Matthew Meredith,[2] Ryan Morshead,[2] Juan A. Muniz,[2] Sandeep Narayanaswami,[2] Ciro Nishiguchi,[2] Timothy Paule,[2] Kelly A. Pawlak,[2] Kristen L. Pudenz,[2] David Rodríguez Pérez,[2] Jon Simon,[2,5] Aaron Smull,[2] Daniel Stack,[2] Miroslav Urbanek,[2] René J. M. van de Veerdonk,[2] Zachary Vendeiro,[2] Robert T. Weverka,[2] Thomas Wilkason,[2] Tsung-Yao Wu,[2] Xin Xie,[2] Evan Zalys-Geller,[2] Xiaogang Zhang,[2] and Benjamin J. Bloom[2]

[1] *Microsoft Azure Quantum*
[2] *Atom Computing*
[3] *Department of Electrical and Computer Engineering, University of Southern California*
[4] *Department of Physics, Colorado School of Mines*
[5] *Department of Physics and Department of Applied Physics, Stanford University*

Transitioning from quantum computation on physical qubits to quantum computation on encoded, logical qubits can improve the error rate of operations, and will be essential for realizing valuable quantum computational advantages. Using a neutral atom quantum processor with 256 qubits, each an individual Ytterbium atom, we demonstrate the entanglement of 24 logical qubits using the distance-two $[\![4, 2, 2]\!]$ code, simultaneously detecting errors and *correcting* for lost qubits. We also implement the Bernstein-Vazirani algorithm with up to 28 logical qubits encoded in the $[\![4, 1, 2]\!]$ code, showing better-than-physical error rates. We demonstrate fault-tolerant quantum computation in our approach, guided by the proposal of Gottesman (2016), by performing repeated loss correction for both structured and random circuits encoded in the $[\![4, 2, 2]\!]$ code. Finally, since distance-two codes can correct qubit loss, but not other errors, we show repeated loss and error correction using the distance-three $[\![9, 1, 3]\!]$ Bacon-Shor code. These results begin to clear a path for achieving scientific quantum advantage with a programmable neutral atom quantum processor.

I. INTRODUCTION

Quantum computers can enable faster, more accurate solutions than classical computers. However, the biggest challenge to scaling up quantum computers is errors, or "noise." Physical qubits and their operation are inherently noisy. State-of-the-art two-qubit gate error rates depend on the qubit implementation, and in some flagship quantum processors range, e.g., from $p = 0.1\%$ for an ion trap processor [MBA+23] to an average of $p = 0.4\%$ for a superconducting qubit processor [GC24]. If a circuit cannot tolerate errors, it can only run for roughly $1/p$ steps, or fewer, which is not nearly enough to achieve large-scale, advantageous computation. Even the best physical qubits are insufficiently reliable, without error correction, to run even moderate-size quantum algorithms.

Indeed, obtaining a quantum advantage in scientific applications will likely require at least 100 qubits with error rate p at most 10^{-6}, while a quantum advantage for industrial-scale problems may require upwards of 1000 qubits with $p \sim 10^{-12}$ [BMT+22]. Such error rates will not be achievable at the physical level. Fortunately, encoding qubits in quantum error-correcting codes, thereby creating "logical" qubits, should allow dramatic reductions in effective error rates. The operations must also be encoded, according to fault-tolerant constructions [AGP06]. Thus, by using quantum error correction and fault tolerance, noise in quantum hardware can be addressed through software, albeit with a cost in physical qubit overhead.

In this work, we present a step toward achieving scientific quantum advantage by demonstrating reliable quantum computation using logical qubits that outperforms corresponding physical-qubit based computation. We present our results on a neutral atom quantum processor. Neutral atom quantum architectures recently have been in rapid development. Previously, neutral atom architectures were predominantly analog in nature. Recent progress has enabled neutral atom approaches to transition to digital, gate-based computation [EBK+23, SST+23, MLP+23, RCC+24, FTS+24, Ato24]. The promise of neutral atoms as qubits is their configurability, both in count and connectivity, while also maintaining low error rates. The neutral atom quantum processor we use in this work has up to 256 qubits (Ytterbium atoms), with all-to-all con-

* These authors contributed equally to this work.

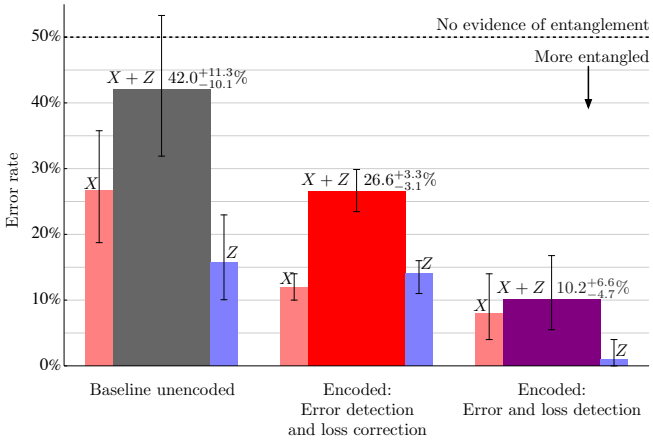

FIG. 1. Summary of results for the 24-qubit cat state. Shown is the error for measurements in the X basis, the error for measurements in the Z basis, and their sum, for three cases. A total less than 50% implies entanglement. The baseline (left) is an unencoded 24-qubit cat state; the error bars are large because we have conservatively chosen only the best run instead of averaging all baseline runs, which would further increase the separation between logical and physical performance. See Fig. 7 for more details. The encoded bars are based on different ways of interpreting the same data for $[\![4, 2, 2]\!]$-encoded cat states. In one case (middle), we reject trials with a detected error, but attempt to correct for lost qubits. In the other case (right), we reject trials with any lost qubit or detected error.

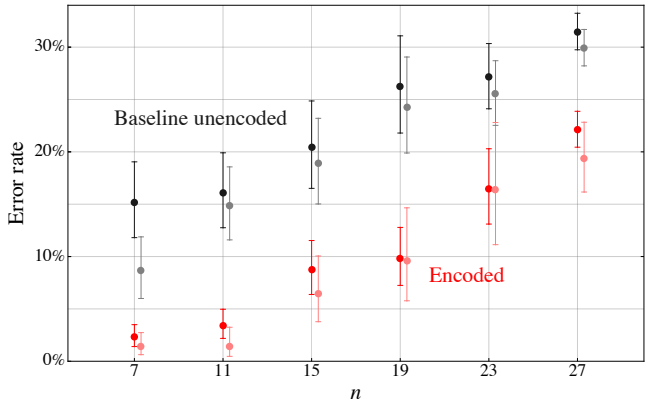

FIG. 2. Summary of results for the Bernstein-Vazirani algorithm with an n-bit secret string. The string is always 1^n, as the corresponding oracle is the most difficult to implement. The success probability is the probability of measuring 1^n, conditioned on acceptance. For the unencoded algorithm (black), we accept when the n measured atoms are present. For the encoded algorithm (red), we accept when all of the n measured code blocks are decodable; in particular, it can detect faults and correct for lost atoms. The lighter points are based only on those trials with no initial atom loss.

nectivity enabled by atom movement, along with high two-qubit physical gate fidelity and atom loss detection. This allows for flexible computation, as well as the ability to both use and optimize over a wide range of quantum error-correcting codes, including those requiring non-local connectivity, for the underlying neutral atom architecture. We refer to the system for detecting and correcting errors, also during computation, as the qubit virtualization system, as encoded, logical qubits are *virtual* qubits made up of some number of physical qubits.

Through co-optimization of fault-tolerant quantum error correction protocols within the qubit virtualization system and the neutral atom quantum processor design, we demonstrate the creation of logical qubits, their logical entanglement, and logical computation, while correcting for lost atoms.

Key results. We demonstrate a variety of reliable quantum computations that outperform physical qubit computation using logical qubits co-designed with a programmable neutral atom quantum processor. First, we show entanglement of 24 logical qubits in a "cat" state (Fig. 1). This is the largest encoded cat state on record to date, illustrating the scale available in neutral atom processors. We then demonstrate quantum algorithms encoded into logical qubit computations. We implement the Bernstein-Vazirani algorithm [BV97, CEMM98], a quantum algorithm well known for showing the higher efficiency of quantum computers versus classical. Our implementations involve as many as 28 logical qubits, encoded in 112 physical qubits (Fig. 2). Next, we demonstrate fault tolerance guided by a proposal of Gottesman [Got16]. These experiments incorporate repeated error detection and, notably, repeated loss *correction*, a critical feature for scaling neutral atom processors. Each of the above experiments are encoded to distance two; they are capable of detecting phase and bit-flip errors and correcting atom loss. Finally, we demonstrate correcting both loss and errors, with repeated error correction in the distance-three Bacon-Shor code [Bac06].

Related work. Creating and verifying large cat states, also known as GHZ states [GHZ89], is a common benchmark for measuring hardware progress [Kre24]. The quality of an experiment is typically expressed by the fidelity with the ideal cat state, and where a fidelity greater than 1/2 is the success criterion. For example, Moses et al. [MBA+23] prepared the 20-qubit cat state with an 86% fidelity, and the 32-qubit cat state with an 82% fidelity, on the Quantinuum H2 trapped-ion processor. Using superconducting qubits, Bao et al. [BXS+24] prepared a 60-qubit cat state with a 59% fidelity. For encoded qubits, the published record to date is an encoded 12-qubit cat state with at least a 99.8% fidelity, also on H2 [RAC+24]. On a neutral atom system, Bluvstein et al. [BEG+24] have prepared a four-qubit encoded cat state with a fidelity of 72(2)% using error correction, ranging to $99.85^{+0.1}_{-1.0}$% using full error detection and therefore with much lower acceptance probability. Table I summarizes results with encoded cat states.

The Bernstein-Vazirani algorithm for finding a secret string is another benchmark for quantum processors [LGM+24]. It has been implemented with unen-

TABLE I. Experiments preparing encoded cat states.

Reference	Logical qubits	Code	Fidelity
[HDHL24]	4	$[\![25,4,3]\!]$	$99.5^{+0.2}_{-0.4}\%$ to $99.7^{+0.2}_{-0.3}\%$
[BEG+24]	4	$[\![7,1,3]\!]$	72(2)% error correction $99.85^{+0.1}_{-1.0}\%$ error detection
[RAC+24]	12	$[\![16,4,4]\!]$	$99.82^{+0.12}_{-0.4}\%$ to $99.90^{+0.1}_{-0.3}\%$
This work	24	$[\![4,2,2]\!]$	$73.4^{+3.1}_{-3.3}\%$ to $85.6^{+2.3}_{-2.5}\%$ error detection and loss correction $89.8^{+4.7}_{-6.6}\%$ to $91.5^{+4.3}_{-6.2}\%$ error and loss detection

coded qubits on superconducting processors [RHK+20, DH21, PL23], ion trap processors [FHM+16, DLF+16, WBD+19], and both processor types [LMRM17, MLM+19, BWM21, LJV+23], for various lengths of the secret string, up to length 26 for superconducting qubits [PL23] and up to length 20 for ion traps [LJV+23]. It is difficult to compare these results fairly. Some test identification of the secret $s = 1^n$, since it is hardest to implement; the corresponding oracle requires the most two-qubit gates. Others test against random strings s or average over different Hamming weights, and this is much easier, particularly on ion traps, comparable to finding $s = 1^{n/2}$. The success probabilities also vary considerably, e.g., from an exponentially small value for random s with length 26 [PL23], to 70% for random s with length 20 [LJV+23].

A critical capability for enabling more complex, reliable computation in a quantum processor is repeated detection and correction of errors. The latest generations of quantum hardware have enabled a variety of such demonstrations within the past few years. Repeated error detection with distance-two codes has been demonstrated on ion traps, including three rounds on eight logical qubits [SBA24], and 15 rounds on four logical qubits [YDKR24]. Demonstrations based on Gottesman's protocol [Got16] for fault tolerance with the $[\![4,2,2]\!]$ code, but without including repeated error detection, include [WWJ+18, HF19, Vui18, LGL+17, CCNH21].

Repeated error correction, with higher-distance codes, has also been demonstrated. For single logical qubits, demonstrations include those on trapped-ion processors [RBL+21, PBP+24] and superconducting processors [KLR+22, Goo23, GC24, PNH+24] each with varying numbers of rounds, e.g., up to nearly 36 rounds of error correction (250 syndrome extraction cycles) on the $[\![49,1,7]\!]$ surface code, with a 0.143(3)% logical error rate per cycle [GC24]. Repeated error correction on multiple qubits has been implemented, including three rounds on two logical qubits [PSR+24], and five rounds on eight logical qubits [RAC+24], each while beating error rates of physical baselines.

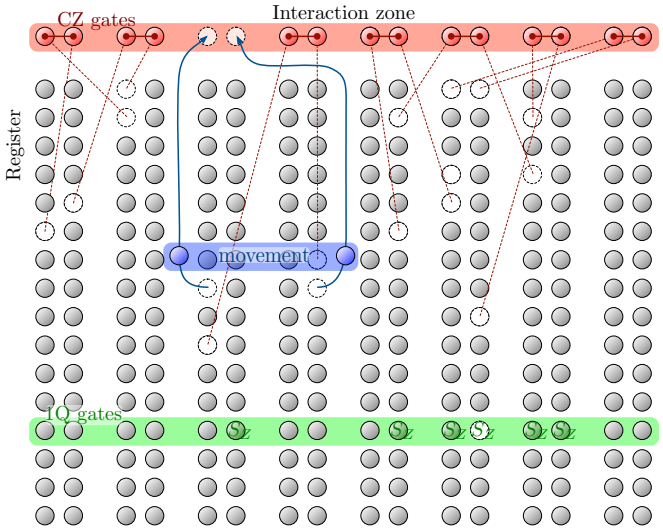

FIG. 3. Diagram of experimental architecture. ^{171}Yb atoms, which each encode a physical qubit in their ground-state nuclear spin, can occupy tweezer traps within either a register array or an interaction zone (IZ). Up to 8 pairs of atoms interact at a time in the IZ, driven by two-qubit (2Q) gate lasers to implement controlled phase gates on the atoms in each pair. Arbitrary single-qubit (1Q) operations can be applied in parallel to the atoms within a row of the register; here one atom is missing. Each atom has a home register location, indicated by dashed lines, where it is originally loaded and where 1Q gates can be applied. Movement of atoms between the two zones enables arbitrary connectivity for 2Q gates. Up to eight atoms from the same row can move in parallel, but their paths cannot cross.

II. PHYSICAL MACHINE DESCRIPTION

All results presented in this work were obtained on a quantum processor based on reconfigurable arrays of neutral ^{171}Yb atoms, depicted in Fig. 3, with the qubits encoded in the ground-nuclear spin states ($^1S_0$, $m_F = \pm 1/2$). Aspects of the system have previously been described in [BBB+22, NC+23, NKC+24], as well as an accompanying publication [Ato24]. Further system and benchmarking details will follow in a separate manuscript, in preparation.

By moving atoms between arrays of static optical tweezer traps using mobile tweezers, this platform enables arbitrary connectivity between qubits, for a large numbers of qubits. Single-qubit operations and qubit storage are performed in a register array, which is loaded in an iterative manner from a repeatedly filled reservoir [NKC+24]. Two-qubit gates are performed in a separate interaction zone (IZ). For this work, up to 256 atoms are available for computation, and up to eight atoms within the same row may be moved between the register and IZ at a time, subject to constraints associated with intermodulation in the acousto-optic deflectors used to generate the moving tweezers. Typical atom loss probabilities per move are below 0.1%. State-resolved, low-loss readout is performed

by transferring atoms from the tweezer arrays into traps formed by cavity-enhanced optical lattices, which allows for state and atom detection with error and loss rates at the few parts-per-thousand level (see [NKC+24] for a detailed characterization of state preparation and imaging). Importantly, the ability to perform state-selective, low-loss imaging allows us to distinguish between different types of error. An image performed prior to circuit execution allows the identification of sites successfully occupied by atoms, while a pair of images directly after circuit execution and after optical pumping within the qubit subspace allow determination of both the presence and state of the atoms.

In the encoded Bernstein-Vazirani experiment with $n = 7$, for example, on average 0.52(7)% of the 32 atoms were not loaded, and 1054 of 1200 shots, or 85(2)%, had no initial loss. The fraction of qubits lost during the circuit averaged $2.3^{+0.2}_{-0.1}$%. Initial loss varies, and more complicated circuits would have a higher circuit loss rate.

Single-qubit operations are performed in parallel on rows of atoms within the register, with the pulse area, phase, and presence of the gates controlled individually on each site using an architecture similar to that described in Ref. [BBB+22]. These gates are performed using two-photon Raman transitions driven by two independently controlled and site-resolved laser beams detuned roughly 10 GHz from the $^3\mathrm{P}_1$, $F = 1/2$ manifold. We calibrate an S_X gate on each site of the register, and perform virtual Z rotations of arbitrary angle by changing the relative phase of the two drive lasers on subsequent gates. We characterize the performance of the single-qubit operations using a Clifford randomized benchmark sequence. At depths of up to 500 Clifford gates, we find an average fidelity of 99.85(2)% per Clifford gate, averaged across three rows of the register spanning those used in this work. Because the nuclear spin qubit is well-isolated from differential light-shifts and has low sensitivity to magnetic fields, we do not automatically apply dynamical decoupling sequences for the circuits presented in this work.

Two-qubit controlled-phase (CZ) gates are performed in the IZ on up to eight pairs of atoms in parallel. These gates are mediated by excitation to a highly-excited Rydberg state ($65^3\mathrm{S}_1$). The sites of the IZ are spaced such that atoms occupying the same pair of sites are in the so-called "Rydberg blockade" limit, where the strength of interactions between the atoms exceeds other relevant energy scales, while atoms in different pairs interact weakly enough to be treated independently. All operations in the IZ are applied in parallel to all atoms within the IZ.

Atoms are excited to the Rydberg state using a sequential two-photon transition. State-selectivity is provided by the first stage of the two-photon transition, from $^1\mathrm{S}_0$, $m_F = -1/2$ to the metastable $^3\mathrm{P}_0$, $m_F = 1/2$ state. Polarization selectivity, along with the narrow linewidth of the transition and slow Rabi rate (10 kHz) relative to the qubit frequency (376 kHz) ensure that only one qubit state is excited to the metastable state. From the metastable state, atoms are excited to the Rydberg state using a UV laser pulse (total duration 110 ns) that implements a gate similar to the time-optimal controlled-phase (CZ) gate described in [JP22]. While the IZ traps are equally confining for the ground and metastable states, the register traps are near a tune-out wavelength for the metastable states, providing near-zero trapping potential. Thus, any gate errors that lead to population being left in the metastable state (such as some coherent population errors on either stage of the two-photon transition) are converted to loss and can be detected. This "erasure conversion" proves useful in identifying the location of errors [WKPT22].

TABLE II. Randomized benchmark infidelities, post-selected on an atom (1Q) or pair of atoms (2Q) remaining in the qubit subspace, and probability of one or both atoms being lost from the qubit subspace. Benchmarking sequences are described in the main text.

Benchmark protocol	Infidelity	Loss + Leakage
1Q Clifford RB	0.15(2)%	0.007(1)%
2Q Static IRB	0.56(15)%	0.27(6)%
2Q Echoed RB with moves	0.4(1)%	0.5(1)%
2Q Echoed RB without moves	0.35(5)%	0.24(6)%

We quantify the performance of our two-qubit gates using several variations on randomized benchmarking. In all presented cases, data is taken in parallel over the eight pairs of sites in the IZ, and averaged. To isolate the performance of the two-qubit gates themselves, in the absence of any errors that may be incurred through atomic movement, we perform interleaved randomized benchmarking (IRB) on static atoms within the IZ. In this protocol, we compare the return probability after a given number of random two-qubit Clifford operations (plus a return pulse calculated to return to a desired measurement state) to the same circuit with an additional CZ gate interleaved after each Clifford gate (and with an appropriately modified return pulse). By comparing the probability of returning to the measurement state versus the depth of the Clifford circuit with and without the added CZ gates, we isolate the error associated with the CZ gate alone, averaged over the two-qubit Hilbert space. Here, the atoms are kept in the IZ for all operations (unlike typical circuits, single qubit gates are applied in the IZ for this protocol). Fits to IRB data taken out to depth 34 indicate an infidelity per CZ gate of 0.56(15)% and additional loss and population leakage outside of the qubit subspace of 0.27(6)%.

In actual circuits, atoms are moved between the register and IZ between single-qubit operations and two-qubit operations, to allow arbitrary connectivity. Because atom movement can cause heating, which may impact the performance of all following gates, IRB does not cleanly isolate the performance of the CZ gate when atoms are moved between arrays. For this, we rely on a variant of randomized benchmarking described in [Ato24] and similar to that in [EBK+23], where concatenated circuit

blocks each consist of a random single-qubit operation and two CZ gates separated by an echo pulse. A final gate sequence returns atoms to the measurement basis. We isolate the contribution from the two-qubit gates (along with any loss or infidelity due to associated movements, up to single-qubit phases which are canceled by the echo pulses) by subtracting the per-depth infidelity associated with the single-qubit operations. From this, we extract a per-CZ gate error of 0.4(1)% and loss of 0.5(1)%. For comparison, the same procedure applied to atoms that remain static in the IZ for all operations yields a per-gate error rate of 0.35(5)% and loss of 0.24(6)%. Table II summarizes the results of these benchmarks. The performance of our gates is sensitive to relative alignment of gate lasers and optical potentials, and other factors that may drift on the timescale of hours to days. The values presented here represent typical values over the time period in which the circuits presented in this work were run.

In our experiments, atom movement is scheduled using a combination of manual and algorithmic techniques, including the use of graph and annealing algorithms to minimize the number of atom movement operations.

III. FOUR-QUBIT CODES

The $[\![4,2,2]\!]$ code [VGW96, GBP97] is a stabilizer code [Got98] with stabilizer generators

$$\begin{array}{cccc} X & X & X & X \\ Z & Z & Z & Z \end{array}$$

and logical operators

$$\begin{aligned} \overline{X}_1 &= X\ X\ I\ I \\ \overline{Z}_1 &= I\ Z\ I\ Z \\ \overline{X}_2 &= X\ I\ X\ I \\ \overline{Z}_2 &= I\ I\ Z\ Z \end{aligned}$$

The code can detect any single-qubit error; for example, a single-qubit Y error flips both stabilizer generators. The code can *correct* for a single-qubit loss. For example, if the second qubit is lost and this is known (an erasure error), then logical qubit 1 can still be decoded using the logical operators $\overline{X}_1 \sim IIXX$, $\overline{Z}_1 \sim ZIZI$, because, having multiplied by a stabilizer, these operators are not supported on the second qubit. However, once a qubit is lost, the code does not protect against errors on the remaining qubits, e.g., with the second qubit lost an X_1 qubit error results in a logical $\overline{X}_1$ error.

Observe that encoded $|00\rangle$ is the four-qubit cat state $\frac{1}{\sqrt{2}}(|0000\rangle + |1111\rangle)$. As shown in Figs. 4 and 5, an extra ancilla qubit is needed to prepare this state fault tolerantly [Sho96].

The $[\![4,1,2]\!]$ code is actually the same code, but only using one of the two logical qubits. The other logical qubit is treated as a gauge qubit, meaning we can set it arbitrarily [Bac06]. Unlike the $[\![4,2,2]\!]$ code, the $[\![4,1,2]\!]$ code can sometimes correct two qubit losses. For example, $\overline{X}_1$ can still be decoded if both qubits 1 and 2 are lost, or both 3 and 4, but not any other pair.

Between two $[\![4,2,2]\!]$ or $[\![4,1,2]\!]$ code blocks, transversal physical CNOT gates fault-tolerantly implement logical transversal CNOT. Other logical operations can also be executed fault tolerantly on a $[\![4,2,2]\!]$ code block, including SWAP, CNOT, CZ and Hadamard ($H\otimes H$) on both qubits. Swapping the middle two physical qubits swaps the logical qubits. Swapping the first and third physical qubits implements a logical CNOT gate from 1 to 2. Applying the Hadamard gate H transversally implements logical $H \otimes H$ and a logical swap. Letting $S_Z = \left(\begin{smallmatrix} 1 & 0 \\ 0 & i \end{smallmatrix}\right) = \sqrt{Z}$, and $S_X = \frac{1}{\sqrt{2}}\left(\begin{smallmatrix} 1 & -i \\ -i & 1 \end{smallmatrix}\right) \propto \sqrt{X}$, observe that

$$\begin{aligned} S_Z X S_Z^\dagger &= Y \quad & S_Z Y S_Z^\dagger &= -X \quad & S_Z Z S_Z^\dagger &= Z \\ S_X X S_X^\dagger &= X \quad & S_X Y S_X^\dagger &= Z \quad & S_X Z S_X^\dagger &= -Y. \end{aligned}$$

Simple stabilizer algebra then shows that applying $S_Z \otimes S_Z^\dagger \otimes S_Z^\dagger \otimes S_Z$ implements a logical CZ gate. Finally, using $H = S_Z S_X S_Z$, applying $S_X \otimes S_X^\dagger \otimes S_X^\dagger \otimes S_X$ implements a logical dual CZ gate, $(H \otimes H)\,\mathrm{CZ}\,(H \otimes H)$.

IV. ENCODED 24-QUBIT CAT STATE

An n-qubit cat state can be written as $\frac{1}{\sqrt{2}}(|0^n\rangle + |1^n\rangle)$. Here, we prepare an encoded cat state on 24 logical qubits, encoded with the $[\![4,2,2]\!]$ code into 48 physical qubits. The circuit we implement is explained in Fig. 4. Starting with a logical circuit to prepare $\frac{1}{\sqrt{2}}(|0^{24}\rangle + |1^{24}\rangle)$, we fault-tolerantly encode it into the $[\![4,2,2]\!]$ code. We then arrange the qubits, four code blocks in each row with the ancilla qubits at the end, and schedule the gates and qubit movements as in Fig. 5. The unencoded baseline experiment prepares a 24-qubit cat state using a separately optimized circuit, in Fig. 6.

The cat state has genuine multipartite entanglement, meaning that it is entangled across every bipartition of the n qubits. Any state that has fidelity greater than 1/2 with the ideal cat state also has genuine multipartite entanglement [GS10]. However, states with $\leq 1/2$ fidelity may not even be entangled; the classical mixture $\frac{1}{2}(|0^n\rangle\langle 0^n| + |1^n\rangle\langle 1^n|)$ has fidelity 1/2 with the ideal cat state, but no entanglement. Our experiments, as well as [HDHL24, RAC+24], measure X basis and Z basis error rates, p_X and p_Z. The fidelity to the ideal cat state is between $1 - p_X - p_Z$ and $1 - \max(p_X, p_Z)$, essentially because possible Y errors contribute to both p_X and p_Z; this is the reason for the fidelity ranges in Table I.

We find that for the encoded cat state, using error detection and loss correction, $p_X + p_Z = 26.6^{+3.3}_{-3.1}\%$, while for the unencoded baseline $p_X + p_Z = 42.0^{+11.3}_{-10.1}\%$. The results are summarized in Fig. 1 and Table III. While the encoding is clearly beneficial, interestingly, it helps reduce p_X much more than p_Z. The baseline error bar

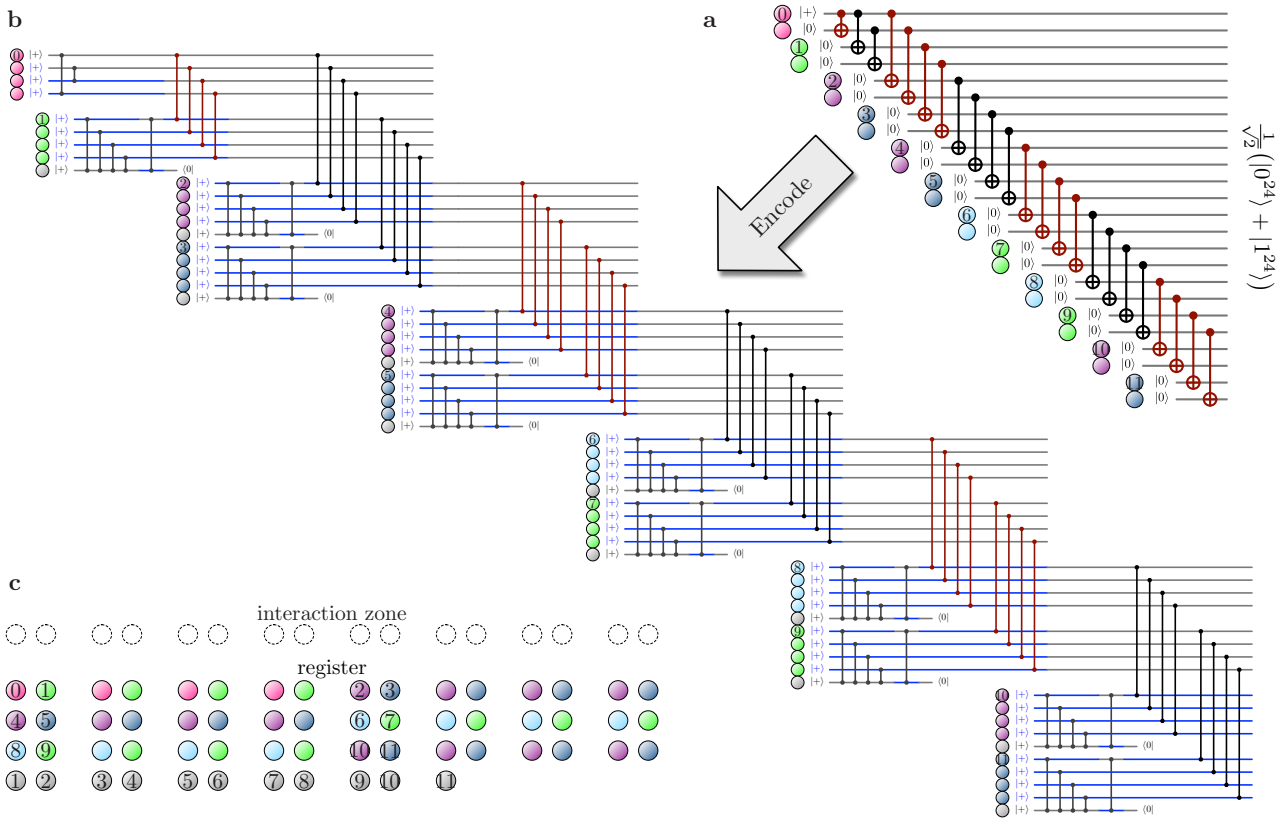

FIG. 4. **(a)** Logical circuit to prepare a 24-qubit cat state $\frac{1}{\sqrt{2}}(|0^{24}\rangle + |1^{24}\rangle)$. The qubits are arranged in 12 pairs that will each be encoded into a $[\![4, 2, 2]\!]$ code block. The logical CNOT gates are applied in seven rounds, indicated by the alternating colors. **(b)** The same circuit, fault-tolerantly encoded into the $[\![4, 2, 2]\!]$ code. This circuit prepares an encoded 24-qubit cat state, and is what runs on the device. The circuit involves 59 atoms (qubits) and 101 physical CZ gates, with a CZ depth of 11; at most five CZ gates touch any qubit. There are 12 code blocks, all but the first using an extra ancilla qubit, shown in gray, to prepare the initial state, encoded $|00\rangle$, fault tolerantly. Each ancilla should be measured to be 0. In the circuit diagram, a blue wire indicates a qubit in the Hadamard basis, and changing in or out of this basis uses a Hadamard gate, not shown. The CZ gates are shown in the correct temporal order, except that the black and red CZ gates are applied in parallel, up to eight at a time. Not shown is that in fact all qubits are together prepared in $|0\rangle$ initially, and only converted to $|+\rangle$ using a Hadamard gate just in time for their first CZ gate. Also not shown are the final transversal X or Z measurements, made simultaneously. **(c)** Arrangement of atoms for the experiment. Each of the top three rows in the storage zone has four code blocks, and the fourth row has the ancilla qubits for blocks 1–11. Not to scale.

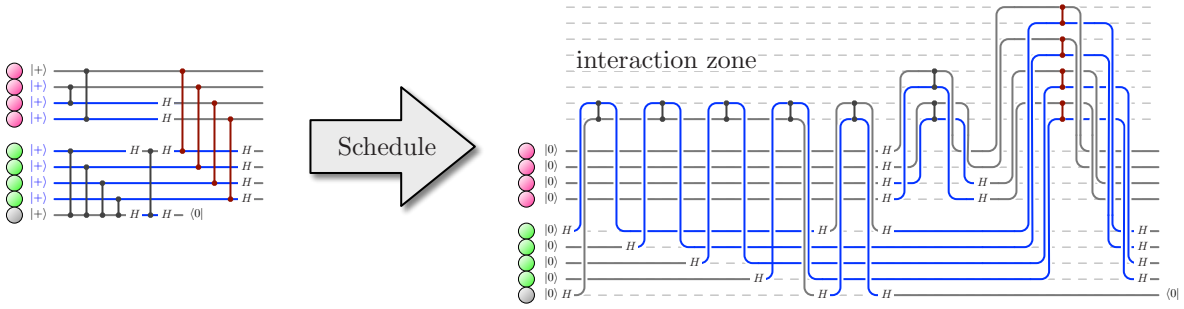

FIG. 5. A portion of the encoded circuit from Fig. 4 prepares an encoded four-qubit cat state. The gates in this circuit need to be scheduled. Two-qubit CZ gates are applied in the interaction zone, up to eight gates in parallel, and all the one-qubit gates on a particular qubit are applied at its initial location in the storage zone. One-qubit gates on a subset of qubits in the same row can be applied in parallel. Two atoms can be moved in parallel, but their paths cannot cross. Note that in this example, for clarity the two code blocks are arranged adjacent to each other in the storage zone, whereas in Fig. 4 they are interleaved.

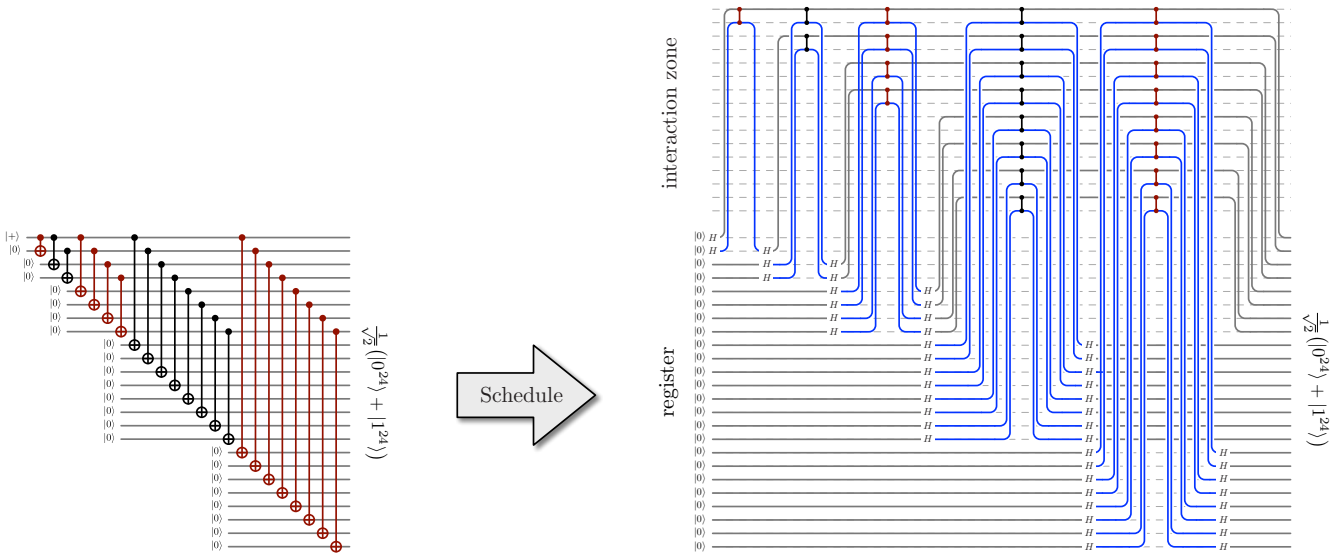

FIG. 6. Circuit to prepare a 24-qubit cat state, unencoded. One-qubit gates are applied at an atom's home register location.

is large because rather than averaging over all trials, we chose for a challenging baseline the best of 27 separate runs, each consisting of 300–400 unencoded trials with X and Z basis measurement; Fig. 7 gives more details.

Figure 8 shows how conditioning on at most k lost qubits, for various values of k, allows a smoother interpolation, in both acceptance probability and total error probability, between the different results in Table III. Finally, Fig. 9 shows the different machine runs that combine to give the data in Table III, plotted conditioned on no initial atom loss. The spread and correlations in the figure suggest some machine parameter drift.

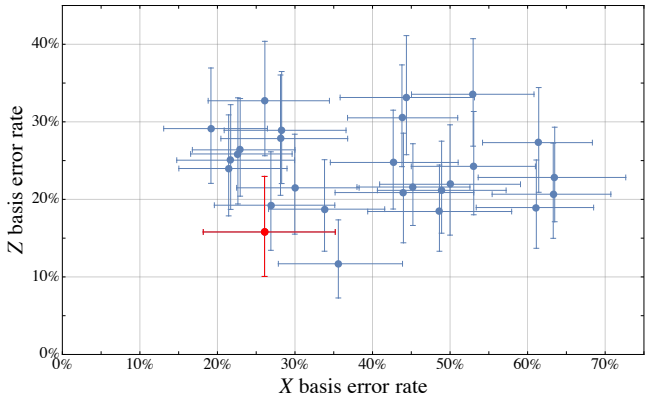

FIG. 7. Each trial of the unencoded baseline 24-qubit cat state experiment included two cat states, one measured in the X basis and the other measured in the Z basis. Shown here are the baseline runs, each consisting of 300–400 trials. Only cat states with no qubit loss are included, on average 135.3 and 161.0 trials for X and Z basis measurements, respectively. The high variance in the observed error rates complicates reporting a single baseline X plus Z basis total error rate. To be conservative, *disadvantaging* the encoded cases, we decided to report the best single run as a baseline. The red data point has the least total error. In the X basis, 26 out of 100 cat states had a logical error, and in the Z basis, 19 out of 121 cat states had a logical error. The baseline error bars in Fig. 1 are large because they are based on only this run, rather than on the average of all the runs in this plot.

V. ENCODED BERNSTEIN-VAZIRANI ALGORITHM

Consider a black box oracle $\{0,1\}^n \to \{0,1\}$, with a secret string $s \in \{0,1\}^n$, that on query x returns $s \cdot x = s_1x_1 \oplus \cdots \oplus s_nx_n$, with $\oplus$ denoting addition modulo 2. Classically, n queries to the oracle are required and sufficient to learn s. The Bernstein-Vazirani algorithm [BV97, CEMM98] makes a single query to the quantum version of this oracle, $U_s = \sum_{x\in\{0,1\}^n, b\in\{0,1\}} |b \oplus (s\cdot x)\rangle\langle b| \otimes |x\rangle\langle x|$, to learn s through the following steps:

$$|-,+^n\rangle \overset{U_s}{\longmapsto} \frac{1}{\sqrt{2^n}} \sum_{x\in\{0,1\}^n} (-1)^{s\cdot x}|-,x\rangle \overset{I\otimes H^{\otimes n}}{\longmapsto} |-,s\rangle \ .$$

This classic algorithm was designed to prove an oracle separation between the classical randomized and quantum polynomial-time complexity classes BPP and BQP.

For $n \in \{7, 11, 15, 19, 23, 27\}$, we implement the Bernstein-Vazirani algorithm for the hardest secret string, $s = 1^n$. We implement the algorithm using $[\![4, 1, 2]\!]$-encoded logical qubits, as well as corresponding unencoded baseline circuits. Figure 10 shows the encoded circuit for $n = 19$, involving $n + 1 = 20$ logical qubits, $4(n + 1) = 80$ atoms and $6n + 2 = 116$ physical CZ gates. The largest instance run, $n = 27$, contains 28 logical qubits, 112 atoms and 170 physical CZ gates. Note that

TABLE III. Data for the 24-qubit cat state experiments. An experiment is accepted if it is neither prerejected nor postrejected. For the encoded experiments, a trial is "prerejected" if it is rejected during the initial state preparation because one of the $|\overline{00}\rangle = \frac{1}{\sqrt{2}}(|0^4\rangle + |1^4\rangle)$ states fails verification. A surviving trial is "postrejected" if a code block cannot be decoded, either because of a detected error or because of two or more lost qubits in the block. We have also filtered out the encoded data with no initial losses, and the data with no losses at all. For the unencoded baseline, a trial is prerejected if there are any initial losses and a surviving trial is postrejected if there are any circuit losses. As explained in Fig. 7, we have selected the best of the unencoded runs, in order to create a challenging baseline.

Experiment	Basis	Trials	Prerejected	Postrejected	Pr[accept]	Errors	Error rate
Cat-24 encoded: all data	X	14 400	10 159	3026	$8.4^{+0.5}_{-0.4}\%$	148	12(2)%
	Z	15 360	11 090	3283	6.4(4)%	170	17(2)%
no initial loss	X	8433	5371	2122	11.1(7)%	115	12(2)%
	Z	8575	5589	2185	9.3(6)%	115	$14^{+3}_{-2}\%$
no loss	X	395	66	221	$27^{+5}_{-4}\%$	9	$8^{+6}_{-4}\%$
	Z	463	98	220	31(4)%	2	$1^{+3}_{-1}\%$
Cat-24 unencoded baseline	X	300	87	113	33(5)%	26	$26^{+8}_{-9}\%$
	Z	300	82	97	$40^{+6}_{-5}\%$	19	$16^{+7}_{-6}\%$

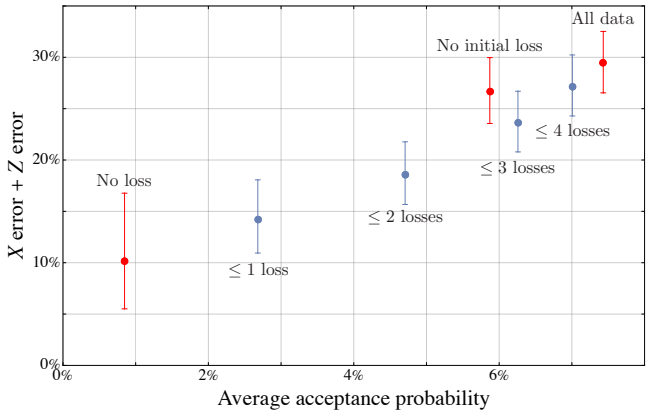

FIG. 8. Data from the encoded 24-qubit cat state experiment, selecting only trials within specified loss criteria. In general, attempting to correct for more loss leads to a higher acceptance probability, but also a higher error rate. In each trial, an atom may be missing before the circuit even begins, a loading loss, or it may be lost during the circuit. The red points show the total X basis plus Z basis error rate, plotted against the average of the X and Z acceptance probabilities, based on either all 29 760 trials, only those 17 008 trials with no initial loss, or only those 858 trials with no loss at all. For the blue points, we select only trials in which the total number of lost qubits, including load loss and circuit loss, is at most a certain threshold. Note that Fig. 9 only includes trials with no initial loss, and the acceptance probabilities in Fig. 9 are conditioned on no initial loss, so the normalization is different. (Figure 7 for the baseline only includes trials with no loss at all.)

for the last n code blocks we store information in the first logical qubit $\overline{X}_1, \overline{Z}_1$ of the $[\![4,2,2]\!]$ code, but for the first block we use $\overline{X}_2, \overline{Z}_2$; this allows logical CZ to be implemented transversally without any qubit swaps. Also, we encode $|+\rangle$ as $|\overline{+1}\rangle = \frac{1}{2}(|01\rangle + |10\rangle)^{\otimes 2}$; setting the gauge qubit to $|1\rangle$ allows us to prepare the state fault tolerantly without any verification. We prefer $|\overline{\pm 1}\rangle$ to $|\overline{\pm 0}\rangle = \frac{1}{2}(|00\rangle \pm |11\rangle)^{\otimes 2}$ because expanded in the computational basis all the terms in $|\overline{\pm 1}\rangle$ have Hamming weight two, making it a decoherence-free subspace invariant to collective dephasing [PSE96].

The unencoded algorithm accepts if no measured atom is lost, and is successful if the measured string is 1^n. The encoded algorithm tolerates losses, but rejects if any of the last n code blocks is not decodable.

Figure 2 summarizes the results, with more details in Table IV. The encoded algorithms have a statistically significantly higher success probability than the unencoded baseline, albeit with a lower acceptance rate.

Computing the success probability conditioned on acceptance makes sense if we treat the Bernstein-Vazirani algorithm as a generic quantum algorithm, as done above. However, it was originally proposed as a quantum *query* algorithm, in which minimizing the number of oracle queries was of key importance. In this light, we can look at the data and ask whether with only one oracle query allowed (one trial), the encoded circuit still beats the unencoded circuit. In short, the answer is probably not. In this case, neither the encoded nor unencoded algorithms can condition on acceptance, and with only one trial it requires guessing the secret string. In particular, with a lost unencoded qubit or an undecodable code block the probability of guessing the corresponding bit is only 1/2, and the expected Hamming distance of the guess away from the secret string increases by 1/2. As shown in Table V, if you are only allowed to make one query to either the unencoded or encoded oracles, and if your goal is to maximize the probability of guessing the secret string s, then for $n \geq 11$ it is better to use the unencoded oracle. On the other hand, if your goal is to minimize the expected Hamming distance of your guess from s, then it is better in all cases to use the encoded oracle.

These statements are not contradictory. They hold because the failure modes of the encoded and unencoded algorithms are quite different, as shown in Fig. 11. Intuitively, an error on the ancilla qubit in the unencoded

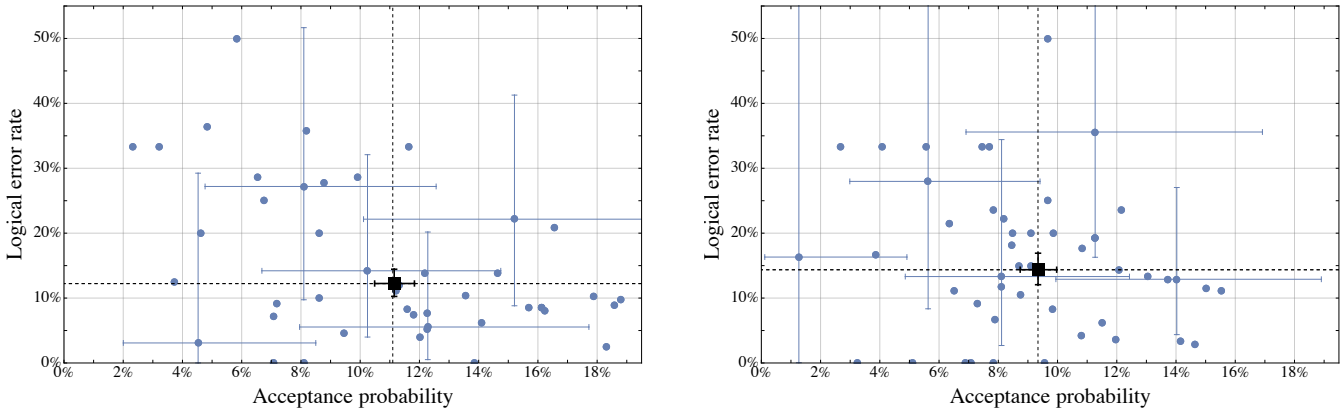

(a) X basis runs (b) Z basis runs

FIG. 9. Encoded 24-qubit cat state data from 45 X basis measurement runs, and 48 Z basis measurement runs. This data was taken overnight, while the machine ran unattended. Each blue point gives the acceptance probability, conditioned on no initial loss, and logical error rate for a run of, on average, 187 trials for the X basis data, and 179 trials for the Z basis data. (We attempted 320 trials, but some trials failed to load all atoms.) For clarity, only some error bars are shown. The black squares are the averages over all the data, the numbers we report. We interpret the negative correlation between acceptance probability and logical error rate as evidence of some machine parameter drift between runs, despite automatic recalibrations.

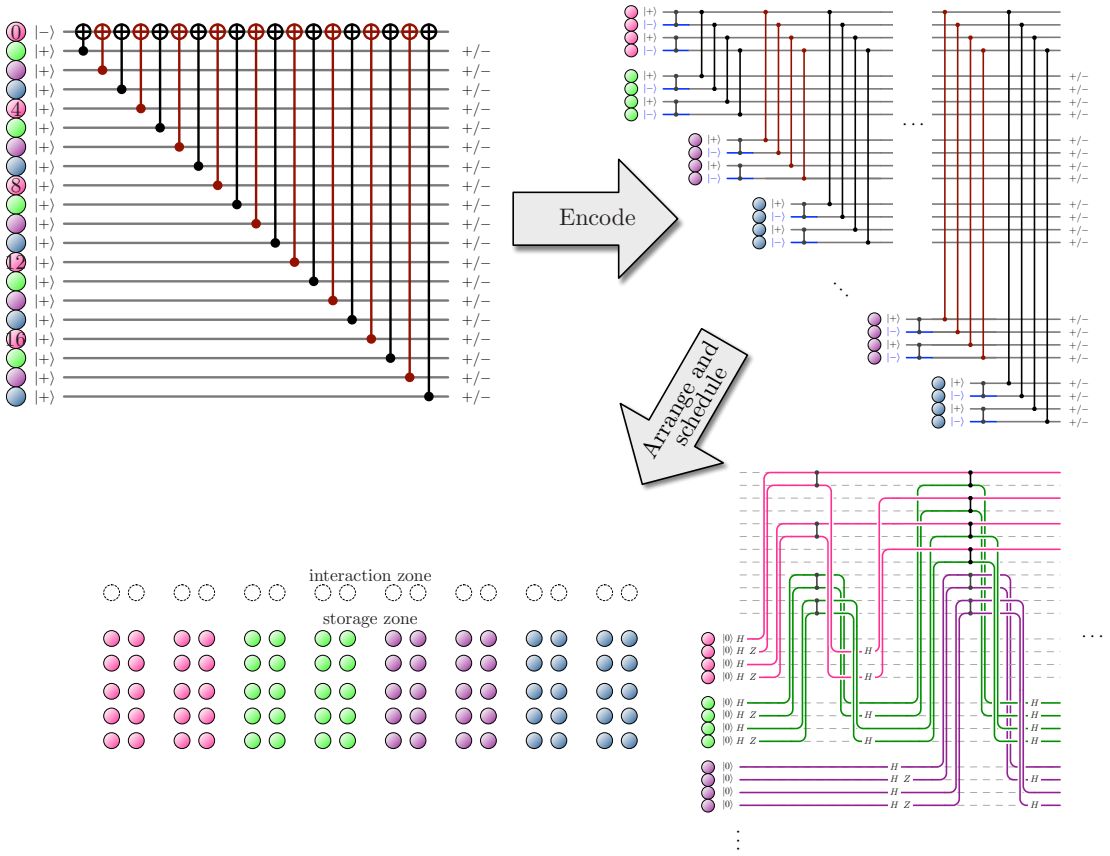

FIG. 10. The $n = 19$ Bernstein-Vazirani algorithm involves $n + 1 = 20$ logical qubits. In our experiment, we test the most challenging case, in which the secret string is 1^n, so there are n logical CNOT gates. Encoded into the $[\![4, 1, 2]\!]$ code, each logical qubit becomes a block of four atoms. There are $4(n + 1)$ atoms and $6n + 2$ physical CZ gates. Four code blocks are arranged in each of the storage zone's top five rows. The gates are scheduled so that the first block, once initialized, stays in the interaction zone. As transversal CZ gates are applied into block j, block $j + 1$ is initialized.

TABLE IV. Data for the Bernstein-Vazirani experiments. The encoded experiment has no preselection. A surviving trial is rejected if one of the last n code blocks cannot be decoded, either because of a detected error or from too many lost qubits. (The first code block is ignored.) For the unencoded baselines, a trial is rejected if a measured qubit is lost.

All data

n	Version	Trials	Rejected	Pr[accept]	Errors	Error rate
7	encoded	1200	409	66(3)%	18	$2.3^{+1.2}_{-0.9}$%
	baseline	600	224	63(4)%	57	15^{+4}_{-3}%
11	encoded	1200	547	54(3)%	22	3^{+2}_{-1}%
	baseline	600	196	67(4)%	65	16^{+4}_{-3}%
15	encoded	1200	740	38(3)%	40	9^{+3}_{-2}%
	baseline	600	243	59(4)%	73	20(4)%
19	encoded	1800	1359	25(2)%	43	11(3)%
	baseline	800	457	43(3)%	90	26^{+5}_{-4}%
23	encoded	2400	1993	17^{+2}_{-1}%	67	16^{+4}_{-3}%
	baseline	3160	2379	25^{+2}_{-1}%	212	27(3)%
27	encoded	26 040	23 789	8.6(3)%	498	22(2)%
	baseline	15 600	12 877	17.5(6)%	857	31(2)%

Trials with no initial loss

n	Version	Trials	Rejected	Pr[accept]	Errors	Error rate
7	encoded	732	233	68(3)%	7	$1.4^{+1.3}_{-0.8}$%
	baseline	425	76	82^{+3}_{-4}%	30	9(3)%
11	encoded	471	181	62(4)%	4	$1.4^{+1.8}_{-1.0}$%
	baseline	540	142	74(4)%	59	15^{+4}_{-3}%
15	encoded	543	308	43(4)%	15	6^{+4}_{-3}%
	baseline	526	176	67(4)%	66	19(4)%
19	encoded	537	369	31(4)%	16	10^{+5}_{-4}%
	baseline	623	289	54(4)%	81	24^{+5}_{-4}%
23	encoded	800	647	19(3)%	25	16^{+6}_{-5}%
	baseline	2173	1409	35(2)%	195	26(3)%
27	encoded	4981	4443	$10.8^{+0.9}_{-0.8}$%	104	19(3)%
	baseline	10 358	7695	25.7(8)%	797	30(2)%

algorithm typically results in a string like $1^{n/2}0^{n/2}$ and contributes on average $n/2$ to the expected Hamming distance from s. On the other hand, an error on the ancilla code block in the encoded algorithm often results in a string like $1^{n/2}\star^{n/2}$, where $\star$ denotes an undecodeable code block where one must guess a bit of s; this contributes only an average of $n/4$ to the expected Hamming distance. Typical errors in the encoded algorithm are heralded, so they contribute less to the expected Hamming distance error metric.

One query to either quantum oracle is much better than one query to the classical oracle. One classical query can only return one bit of s, so the probability of guessing s is $\Pr[\text{guess}] = 1/2^{n-1}$ and the expected Hamming distance to s is $\mathrm{E}[\text{Hamming}] = \frac{n-1}{2}$.

TABLE V. Performance of unencoded and encoded Bernstein-Vazirani algorithms with a single oracle query. Pr[guess] is the probability of guessing the secret string based on the measured outputs, and E[Hamming] the expected distance of the guess away from the secret string. This analysis is based on all trials, including ones with initial loss. For a classical oracle, $\Pr[\text{guess}] = 1/2^{n-1}$ and $\mathrm{E}[\text{Hamming}] = \frac{n-1}{2}$.

	Unencoded baseline		Encoded algorithm	
n	Pr[guess]	E[Hamming]	Pr[guess]	E[Hamming]
7	67(4)%	0.94	75(2)%	0.48
11	69(4)%	1.04	66(3)%	0.90
15	61(4)%	1.58	51(3)%	1.45
19	49(3)%	2.44	38(2)%	2.29
23	35(2)%	3.42	30(2)%	2.97
27	28.2(7)%	4.12	18.5(5)%	4.05

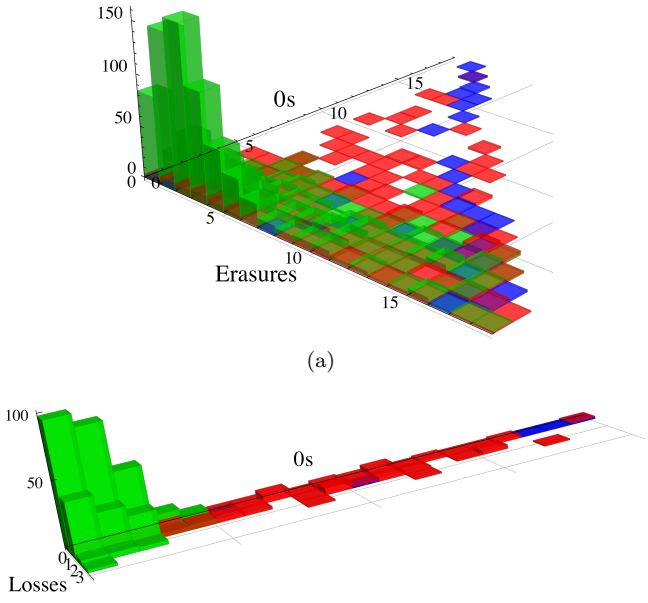

FIG. 11. (a) Histogram of the decoded values for the last n code blocks, for the $n = 19$ encoded Bernstein-Vazirani algorithm. Ideally, every block should decode to 1, with no failed decodings (erasures) or 0s. The green bars are conditioned on the first block decoding to $|-\rangle$, the red bars on it detecting an error, and the blue bars on it decoding to $|+\rangle$, a logical error. Note that when a rare logical error occurs on the first block, the other blocks are mostly corrupted. The analysis in Fig. 2 conditions on the first block decoding to $|-\rangle$, but Table V does not place any conditions on it. (b) Similar histograms for the unencoded baseline algorithm show strikingly different behavior. Qubit losses are rare, regardless of whether the first qubit is $|-\rangle$ (green), lost (red), or $|+\rangle$ (blue). The $[\![4, 1, 2]\!]$ code turns physical errors into erased code blocks.

VI. REPEATED LOSS CORRECTION AND TRANSVERSAL OPERATIONS FOR THE $[\![4,2,2]\!]$ CODE

A. Repeated loss correction with CZ and dual CZ logical gates

The circuits considered so far have only used loss correction and error detection at the very end, when decoding the final measurements. However, it's important to be able to detect and correct errors between computational steps of an algorithm, to enable deeper computation. To that end, we explore using loss correction in the middle of a larger circuit, demonstrating repeated fault-tolerant loss correction. In order to make the circuits more interesting, between rounds of loss correction we apply some of the fault-tolerant logical operations given in Sec. III.

Figure 12 gives a circuit for fault-tolerant error detection for the $[\![4,2,2]\!]$ code. It measures the stabilizer generators $X^{\otimes 4}$ and $Z^{\otimes 4}$ in parallel, with one measurement outcome flagging the other for possible correlated errors. Furthermore, the circuit in Fig. 12(c) replaces two of the data qubits with fresh qubits, so the full data block can be refreshed every two rounds of error detection. This allows us to use the $[\![4,2,2]\!]$ code to correct a lost qubit during a computation, not just at the very end as in our logical cat state procedure.

We design and execute experiments that repeatedly apply logical CZ gates on a $[\![4,2,2]\!]$ code block. Recall that $S_Z \otimes S_Z^\dagger \otimes S_Z^\dagger \otimes S_Z$ implements a logical CZ gate. Error detection with qubit refresh is inserted between each pair of CZ gates, as illustrated in Fig. 13. Note that with $j+1$ logical CZ gates, there are j rounds of error detection, with $5+8j$ CZ gates applied to $5+2j$ qubits.

We also ran a very similar experiment, except applying logical dual CZ gates, $(H \otimes H)\,\mathrm{CZ}\,(H \otimes H)$, using $S_X \otimes S_X^\dagger \otimes S_X^\dagger \otimes S_X$.

The encoded experiments can be compared against corresponding unencoded baselines. Given the system architecture, there are a few reasonable baselines from which to choose. For example, we may choose to return qubits to the storage zone between each CZ, or not. We have chosen to select unencoded baselines in which, as shown in Fig. 13(c), between each pair of CZs or dual CZs, both qubits are moved back to the storage zone and Pauli X or Z gates, respectively, are applied to each of them to cancel coherent dephasing from the movement and two-qubit gates. These baselines performed the best of those that we tried, disadvantaging any comparison between encoded and unencoded.

Results for both repeated logical CZ and repeated logical dual CZ, for up to 10 logical operations and 9 rounds of loss correction, are shown in Fig. 14, with detailed data in Table VI. Since the two physical baselines compile to the same circuit, we have combined them into a single baseline for comparison. The encoded repeated logical CZ experiments largely beat the corresponding baselines, including, for example, an encoded circuit consisting of 10 logical CZs with 9 loss-correction rounds outperforming an unencoded sequence of 10 CZs. Surprisingly, the repeated dual CZ experiment performs much worse for depths 8 and 10. Since it should be similar to repeated CZs, this could be from a mistake in scheduling the circuits, or possibly from machine parameter drift.

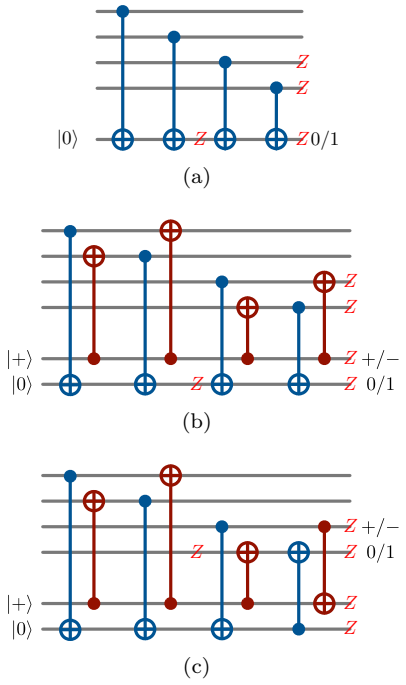

FIG. 12. The top circuit (a) measures the parity of four qubits, i.e., the syndrome of $ZZZZ$. However, it is not fault tolerant; a single Z fault on the ancilla can spread undetected to a weight-two Z error. The next circuit (b) remedies this, and simultaneously measures $XXXX$, using a trick from [Rei20]. Now the bad Z fault will be detected, or "flagged," by the $XXXX$ measurement, and similarly the $ZZZZ$ measurement will flag a bad X fault. This circuit gives an efficient, fault-tolerant error detection procedure for the $[\![4,2,2]\!]$ code. However, it does not correct for a lost qubit. The bottom circuit (c) fixes this, halfway, by switching the direction of the final two CNOT gates. (This is equivalent to inserting swap-based "leakage-detection units" [CBO+24].) The last two data qubits are replaced with fresh ancillas, so in particular if one of them is lost it will be replaced. Thus we can replace all four qubits in two rounds of error detection. Future work will investigate this paradigm by combining mid-circuit measurement, qubit reuse and reinitialization, along with periodic atom cooling to remove a fundamental obstacle to neutral atom quantum computing by limiting the depth of circuit any atom must undergo.

B. Random circuits

As explained in Sec. III, the $[\![4,2,2]\!]$ code allows a variety of other fault-tolerant logical gates. Each of $\{\mathrm{CNOT}, \mathrm{CZ}, \mathrm{SWAP}, H^{\otimes 2}\}$ can be implemented by permutation or transversal gates. This set generates a group

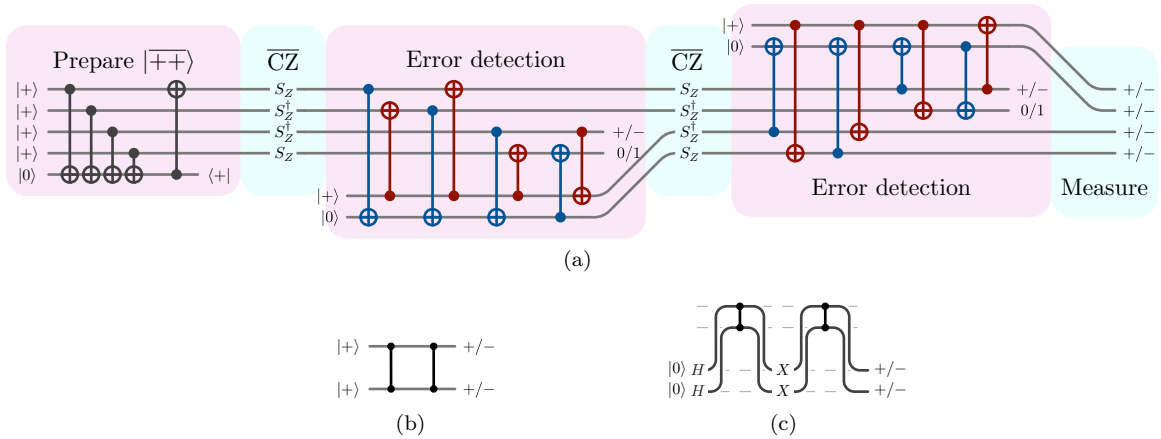

FIG. 13. (a) Encoded circuit that applies two rounds of encoded CZ gates to $|\overline{++}\rangle$, encoded in the $[\![4,2,2]\!]$ code, with two rounds of error detection. Together, the two error detection rounds refresh all four data qubits. (b) The corresponding logical circuit. Since the CZ gates cancel out, both measurements should give $+$. (c) The baseline circuit that we run for comparison. The X echo pulses cancel out coherent dephasing errors from the CZ gates and movement. Both measurements should give $-$. This baseline performs better than applying the two CZ gates sequentially without leaving the interaction zone.

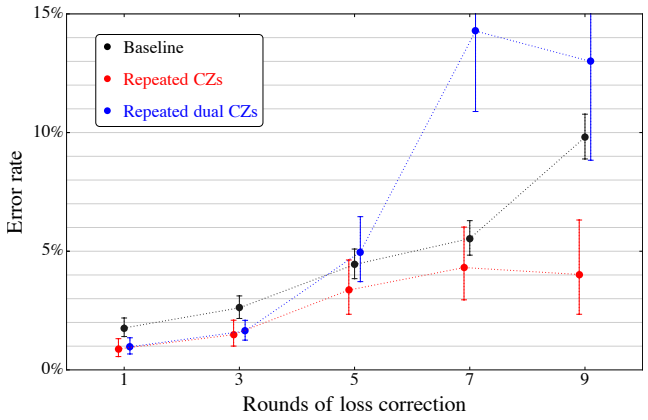

FIG. 14. Error rates for $[\![4,2,2]\!]$ code repeated logical CZ and repeated logical dual CZ experiments, and the corresponding physical baseline, conditioned on no initial loss. Error detection between logical gates (Fig. 13) permits mid-circuit correction of atom loss.

of size 36.

To test the performance of these gates, and in the spirit of Ref. [Got16], we design experiments by preparing encoded $|00\rangle$ and then applying up to four elements of the group at random, with error detection between each pair of elements. The sequences chosen are, using CNOT = CX for brevity:

$$\begin{aligned} 0:&\quad H^{\otimes 2}\,\text{CX} \\ 1:&\quad I,\ \text{CX}\,\text{CZ}\,H^{\otimes 2}\,\text{CX} \\ 2:&\quad H^{\otimes 2}\,\text{SWAP}\,\text{CX},\ \text{CZ}\,H^{\otimes 2}\,\text{SWAP},\ H^{\otimes 2}\,\text{SWAP}\,\text{CZ} \\ 3:&\quad \text{CX}\,H^{\otimes 2}\,\text{CX},\ H^{\otimes 2},\ \text{SWAP}\,\text{CX},\ \text{CZ}\,\text{CX}\,H^{\otimes 2} \end{aligned} \tag{1}$$

The encoding of sequence j involves j rounds of error detection. Note that the error detection circuits used here are those of Fig. 12(b), instead of those of Fig. 12(c); therefore they correct for lost qubits only at the end of the circuit. Future work may include executing these logical operation sequences with the circuits of Fig. 12(c).

The choice to error-detect between group elements is justified by imagining a computation with many [[4,2,2]] blocks. In that scenario, it is natural to write a circuit as alternating layers of CNOTs between blocks, and group elements within each block. It is then also natural to schedule error detection following each pair of layers in order to control the spread of errors among blocks.

The output of each random sequence is a stabilizer state with two generators. Each generator is measured to determine success of failure of the experiment. The encoded circuits can be directly compared to corresponding physical baselines that execute the same gate sequence. Results are shown in Fig. 15, with more details in Table VII. We find the encoded circuits consistently outperform the corresponding physical unencoded baselines.

VII. REPEATED ERROR CORRECTION WITH THE DISTANCE-THREE BACON-SHOR CODE

Running deep logical circuits in a neutral atom quantum computer will ultimately require repeated correction of both errors within the qubit subspace and atom loss from erasure conversion. In order to demonstrate this, we choose the distance-three $[\![9,1,3]\!]$ Bacon-Shor code. This code has previously been implemented on trapped-ion systems [EDN+21, HBC24]. A code distance greater than two is needed to correct errors other than loss.

To our knowledge, the present work is the first demonstration of repeated error correction in neutral atoms. We employ a scheme similar to that of Steane and Knill [Ste97, Kni05, PSR+24], leveraging its ability to

TABLE VI. Data for our $[\![4,2,2]\!]$ repeated controlled-Z and repeated dual controlled-Z experiments. The encoded experiment with CZ or dual CZ depth $k+1$ has k loss-correction rounds. It uses $5+2k$ physical qubits, with $5+8k$ physical CZ gates. A trial is prerejected if the cat state verification fails, and it is postrejected if an uncorrectable error is detected. Results for all available data, and for data in which there is no initial loss are reported separately. The unencoded baseline experiments, the same for CZ as for dual CZ, are on two qubits and include echos to cancel coherent errors. Trials with initial loss are prerejected, and those with circuit loss are postrejected. Restricting to trials with no initial loss has no effect on the baseline.

All data

	CZ or dual CZ depth	Loss-correction rounds	Trials	Prerejected	Postrejected	Pr[accept]	Errors	Error rate
Encoded CZs	2	1	3400	189	732	73^{+1}_{-2}%	34	$1.4^{+0.5}_{-0.4}$%
	4	3	4600	587	2030	43(1)%	43	$2.2^{+0.7}_{-0.6}$%
	6	5	3700	290	2408	27(1)%	41	4(1)%
	8	7	3700	302	2674	20(1)%	37	5^{+2}_{-1}%
	10	9	3700	318	2979	10.9(1)%	21	5(2)%
Encoded dual CZs	2	1	5120	633	1051	67(1)%	53	1.5(0.4)%
	4	3	8640	1388	3340	45(1)%	104	2.7(0.5)%
	6	5	5120	1156	2899	21(1)%	69	6^{+2}_{-1}%
	8	7	5120	1270	3544	$7.7^{+0.8}_{-0.7}$%	63	16^{+4}_{-3}%
	10	9	5120	1640	3242	4.7(6)%	38	16^{+5}_{-4}%
Baseline	2	—	4960	293	302	88.0(9)%	77	1.8(4)%
	4	—	4960	200	431	87.3(9)%	113	$2.6^{+0.5}_{-0.4}$%
	6	—	4960	202	566	84.5(10)%	186	$4.4^{+0.7}_{-0.6}$%
	8	—	4660	202	654	82(1)%	210	$5.5^{+0.8}_{-0.7}$%
	10	—	4960	284	860	77(1)%	374	$9.8^{+1.0}_{-0.9}$%

Trials with no initial loss

	CZ or dual CZ depth	Loss-correction rounds	Trials	Prerejected	Postrejected	Pr[accept]	Errors	Error rate
Encoded CZs	2	1	3119	127	603	77^{+1}_{-2}%	21	$0.9^{+0.4}_{-0.3}$%
	4	3	3787	197	1692	50(2)%	28	$1.5^{+0.6}_{-0.5}$%
	6	5	3209	205	2048	30(2)%	32	3(1)%
	8	7	2890	188	2026	23(2)%	29	4^{+2}_{-1}%
	10	9	3004	210	2417	13(1)%	15	4(2)%
Encoded dual CZs	2	1	4282	333	746	75(1)%	31	$1.0^{+0.4}_{-0.3}$%
	4	3	6732	854	2324	53(1)%	58	$1.6^{+0.5}_{-0.4}$%
	6	5	4064	793	2302	24(1)%	48	5(1)%
	8	7	3626	775	2500	$9.7^{+1.0}_{-0.9}$%	50	14^{+4}_{-3}%
	10	9	3312	940	2171	6.1(8)%	26	13^{+5}_{-4}%

correct atom loss; see Fig. 16. In this work, the ancilla qubits are held until readout at the end of the circuit, so each round of error correction requires the use of additional qubits. However, in principle, this scheme can be combined with mid-circuit measurement and reset where readout and loss detection, combined with mid-circuit reloading, will enable arbitrary-depth circuits.

After one round of error correction, we find a logical error rate of $4.9^{+1.0}_{-0.9}$% and after two rounds the error rate is 8^{+2}_{-1}%. Table VIII gives more details. While these results suggest the opportunity to further improve physical error rates, they also serve as a demonstration of the mechanism to correct for both errors and loss. This can be seen in the analysis of the successful trials with one round of error correction, where on average 0.20 erasures and at least 0.14 errors were corrected in the readout of the final data block, whereas 0.40 erasures and 0.50 errors were corrected in the previous round of X and Z error correction, a higher average number of corrections. In the successful trials with two rounds of error correction, on average 0.22 erasures and at least 0.13 errors were corrected in the readout of the final data block (consistent with the one-round data), while 0.95 erasures and 0.88 errors were corrected in the previous error-correction rounds.

In order to compare encoded and physical results, we must choose a meaningful physical baseline. From the standpoint of the encoded data, the logical circuit is a quantum memory, applying the logical identity operation. For a meaningful comparison, we show results for repeated teleportation of physical qubit states, following the pattern of repeated teleportation of the logical data

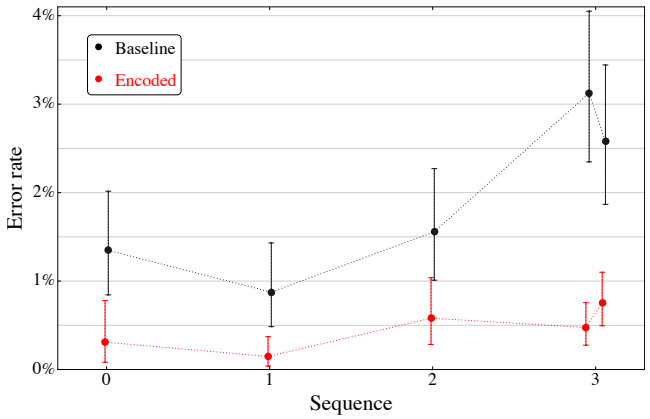

FIG. 15. Error rates for $[\![4, 2, 2]\!]$ code random logical circuits, conditioned on no initial loss. Sequence labels are from the sequences given in Eq (1).

TABLE VII. Data for our $[\![4, 2, 2]\!]$ random circuit experiments. The sequences of operations are specified in Eq. (1). The encoding of sequence k includes k rounds of error detection, $5 + 2k$ physical qubits and $5 + 8k$ physical CZ gates. For sequences 0, 1, and 2, the two stabilizer generators of the output each have weight one and are measured simultaneously in each experiment. An error is reported if either of the two generators have incorrect eigenvalue. The stabilizer generators of sequence 3 are $\{XZ, ZX\}$. The encoded circuit measures both of these generators in the same experiment via transversal Y-basis measurements. The physical baselines require separate experiments for each generator. Results for the two generators are therefore reported separately. All data is reported. Restricting to trials with no initial loss has no effect on the baseline.

All data

	Sequence	Trials	Pre.	Post.	Pr[accept]	Errors	Error rate
Encoded	0	1200	66	42	91(2)%	6	$0.6^{+0.6}_{-0.3}$%
	1	2800	119	467	79^{+1}_{-2}%	5	$0.2^{+0.4}_{-0.1}$%
	2	2500	132	737	65(2)%	9	$0.6^{+0.4}_{-0.3}$%
	XZ 3	7200	595	3292	46(1)%	15	$0.5^{+0.3}_{-0.2}$%
	ZX 3	7200	595	3292	46(1)%	24	0.7(3)%
Baseline	0	1600	52	51	94(1)%	20	$1.3^{+0.7}_{-0.5}$%
	1	1600	40	55	94(1)%	13	$0.9^{+0.6}_{-0.4}$%
	2	1600	66	47	93(1)%	23	$1.6^{+0.7}_{-0.5}$%
	XZ 3	1800	87	108	89(1)%	50	$3.1^{+0.9}_{-0.8}$%
	ZX 3	1800	108	134	87(2)%	40	$2.6^{+0.9}_{-0.7}$%

Trials with no initial loss

	Sequence	Trials	Pre.	Post.	Pr[accept]	Errors	Error rate
Encoded	0	1104	45	35	93^{+1}_{-2}%	3	$0.3^{+0.5}_{-0.2}$%
	1	2645	95	398	81^{+1}_{-2}%	3	$0.1^{+0.2}_{-0.1}$%
	2	2289	105	605	69(2)%	9	$0.6^{+0.5}_{-0.3}$%
	XZ 3	6315	425	2702	50(1)%	15	$0.5^{+0.3}_{-0.2}$%
	ZX 3	6315	425	2702	50(1)%	24	0.8(3)%

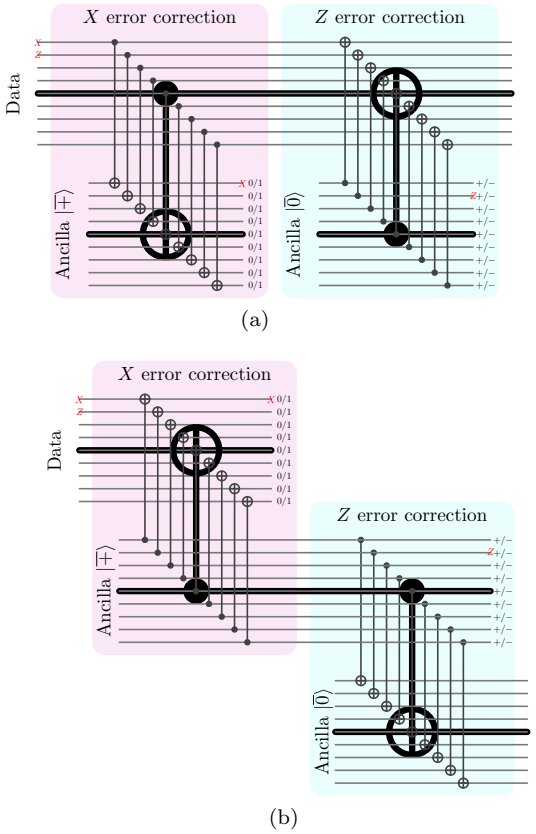

FIG. 16. (a) In Steane's scheme to correct X errors, an ancilla code block is fault-tolerantly prepared in the encoded $|+\rangle$ state. The data block is coupled to it with transversal CNOT gates into the ancillas. This logical CNOT has no logical effect, since $|+\rangle$ is preserved by X (NOT), but it copies X errors to the ancilla block. Measuring the ancillas transversally in the Z basis allows the X errors to be identified and corrected. (Generally, the corrections are not actually applied to the data block, but rather stored classically, as the "Pauli frame" for the data.) Z error correction is symmetrical, using an ancilla block prepared as encoded $|0\rangle$. (b) We modify the scheme so that X and Z error correction are both implemented by logical one-qubit teleportation [ZLC00], thus making a connection to teleportation-based syndrome extraction [Kni05, PSR+24]. This method has the advantage that a lost atom will be refreshed with a new qubit. The logical corrections to complete one-qubit teleportation are not shown above, but are stored in the Pauli frame.

in Fig. 16(b).

VIII. OUTLOOK

In this work, we have created large entangled logical states, implemented computational algorithms on encoded qubits, demonstrated qubit loss correction, and implemented a code with the capacity for repeated loss and error correction. Altogether, these results highlight the unique features and promise of neutral atoms as a platform for reliable fault-tolerant quantum computing.

TABLE VIII. Data for $[\![9, 1, 3]\!]$ Bacon-Shor code repeated error correction (EC) experiments. The data for the encoded circuits includes all trials, including those with initial loss, and there is no preselection. When decoding logical X (Z), a trial is postrejected if there are losses in two or more rows (columns) of the 3×3 code, or if one row is lost and the other two disagree. For the unencoded baseline, a trial is prerejected if there are any initial losses and a surviving trial is postrejected if there are any circuit losses.

Experiment		Physical qubits	Physical CZs	Trials	Prerejected	Postrejected	Pr[accept]	Errors	Error rate
Encoded	1 EC round	27	36	2400	—	541	77(2)%	91	$4.9^{+1.0}_{-0.9}$%
	2 EC rounds	45	66	2400	—	1054	56(2)%	114	8^{+2}_{-1}%
Baseline	2 1Q teleportations	3	2	640	31	47	88^{+2}_{-3}%	7	$1.3^{+1.2}_{-0.7}$%
	4 1Q teleportations	5	4	640	50	82	79(3)%	7	$1.4^{+1.3}_{-0.8}$%

The large encoded cat states and the Bernstein-Vazirani algorithms are enabled by the combination of scalability, high-fidelity operations inherent to neutral atoms, and all-to-all connectivity among the qubits. For larger-scale logical computation, this connectivity paired with high qubit count will enable the use of nonlocal error-correcting codes with high encoding rates and low physical qubit overhead [XZZ+24].

All of the encoded experiments, particularly those with repeated error detection, highlight the usefulness of loss-to-erasure conversion in the context of encoded qubits. They demonstrate that logical circuits can operate effectively with atom loss, which will be a key feature of large-scale neutral atom quantum computers.

This work and similar work with other neutral atom platforms [BEG+24], as well as recent work with superconducting qubits [GC24] and trapped ion qubits [PSR+24, RAC+24], highlight a critical advance in the field of quantum computation: the transition from scientific results computed with physical qubits to computational advances achieved with logical qubits. After a relatively short time the neutral atom platform has shown significant advancement from its inception as an experimental quantum computing platform. In the near future we expect advances in both 2Q gate fidelities as more iterations are performed to reduce gate laser noise as well as significant scale up towards 10 000 qubits allowing for larger distance codes, more performant logical qubits, and more impressive demonstrations of fault-tolerant, universal quantum computation.

The combination of a hardware-optimized qubit virtualization system, complete with high-rate and high-efficiency quantum error correction, with a programmable neutral atom quantum processor, inclusive of mid-circuit measurement [NC+23], continuous atom reloading [NKC+24], and increased two-qubit gate fidelity, is a promising path to achieving large-depth, logical computation for scientific quantum advantage.

ACKNOWLEDGMENTS

We thank Zulfi Alam, David Bohn, Jeongwan Haah, Chetan Nayak, Pasi Kostamo, Vadym Kliuchnikov, Dennis Tom, Matthias Troyer, and Jason Zander for their support and feedback during this project.

[AGP06] P. Aliferis, D. Gottesman, and J. Preskill. Quantum accuracy threshold for concatenated distance-3 codes. *Quant. Inf. Comput.* 6:97 (2006), arXiv:quant-ph/0504218.

[Ato24] Atom Computing, Inc. High fidelity universal gates in the ^{171}Yb ground state nuclear spin qubit. *Submitted November 2024* (2024).

[Bac06] D. Bacon. Operator quantum error correcting subsystems for self-correcting quantum memories. *Phys. Rev. A* 73:012340 (2006), arXiv:quant-ph/0506023.

[BBB+22] K. Barnes, P. Battaglino, B. J. Bloom, et al. Assembly and coherent control of a register of nuclear spin qubits. *Nat. Commun.* 13(1):2779 (2022), arXiv:2108.04790.

[BEG+24] D. Bluvstein, S. J. Evered, A. A. Geim, et al. Logical quantum processor based on reconfigurable atom arrays. *Nature* 626:58–65 (2024), arXiv:2312.03982.

[BMT+22] M. E. Beverland, P. Murali, M. Troyer, et al. Assessing requirements to scale to practical quantum advantage. (2022), arXiv:2211.07629.

[BV97] E. Bernstein and U. Vazirani. Quantum complexity theory. *SIAM J. Comput.* 26(5):1411–1473 (1997).

[BWM21] S. Blinov, B. Wu, and C. Monroe. Comparison of cloud-based ion trap and superconducting quantum computer architectures. *AVS Quantum Sci.* 3:033801 (2021), arXiv:2102.00371.

[BXS+24] Z. Bao, S. Xu, Z. Song, et al. Schrödinger cats growing up to 60 qubits and dancing in a cat scar enforced discrete time crystal. *Nat. Commun.* 15:8823 (2024), arXiv:2401.08284.

[CBO+24] M. N. H. Chow, V. Buchemmavari, S. Omanakuttan, et al. Circuit-based leakage-to-erasure conversion in a neutral atom quantum processor. *PRX Quantum* (2024), arXiv:2405.10434.

[CCNH21] R. Cane, D. Chandra, S. X. Ng, and L. Hanzo. Experimental characterization of fault-tolerant circuits in small-scale quantum processors. *IEEE Access* 9:162996–163011 (2021), arXiv:2112.04076.

[CEMM98] R. Cleve, A. Ekert, C. Macchiavello, and M. Mosca. Quantum algorithms revisited. *Proc. R. Soc. London A* 454(1969):339–354 (1998), arXiv:quant-ph/9708016.

[DH21] M. L. Dahlhauser and T. S. Humble. Modeling noisy quantum circuits using experimental characterization. *Phys. Rev. A* 103:042603 (2021), arXiv:2001.08653.

[DLF+16] S. Debnath, N. M. Linke, C. Figgatt, et al. Demonstration of a small programmable quantum computer with atomic qubits. *Nature* 536:63–66 (2016), arXiv:1603.04512.

[EBK+23] S. J. Evered, D. Bluvstein, M. Kalinowski, et al. High-fidelity parallel entangling gates on a neutral-atom quantum computer. *Nature* 622(7982):268–272 (2023), arXiv:2304.05420.

[EDN+21] L. Egan, D. M. Debroy, C. Noel, et al. Fault-tolerant control of an error-corrected qubit. *Nature* 598:281–286 (2021), arXiv:2009.11482.

[FHM+16] S. D. Fallek, C. D. Herold, B. J. McMahon, et al. Transport implementation of the Bernstein-Vazirani algorithm with ion qubits. *New J. Phys.* 18:083030 (2016), arXiv:1603.05672.

[FTS+24] R. Finkelstein, R. B.-S. Tsai, X. Sun, et al. Universal quantum operations and ancilla-based read-out for tweezer clocks. *Nature* 634(8033):321–327 (2024), arXiv:2402.16220.

[GBP97] M. Grassl, T. Beth, and T. Pellizzari. Codes for the quantum erasure channel. *Phys. Rev. A* 56(1):33–38 (1997), arXiv:quant-ph/9610042.

[GC24] Google Quantum AI and Collaborators. Quantum error correction below the surface code threshold. 2024, arXiv:2408.13687.

[GHZ89] D. M. Greenberger, M. A. Horne, and A. Zeilinger. Going beyond Bell's theorem. In M. Kafatos, editor, *Bell's Theorem, Quantum Theory and Conceptions of the Universe*, Fundamental Theories of Physics, pages 69–72. Springer Netherlands, 1989.

[Goo23] Google Quantum AI. Suppressing quantum errors by scaling a surface code logical qubit. *Nature* 614:676–681 (2023), arXiv:2207.06431.

[Got98] D. Gottesman. Theory of fault-tolerant quantum computation. *Phys. Rev. A* 57:127 (1998), arXiv:quant-ph/9702029.

[Got16] D. Gottesman. Quantum fault tolerance in small experiments, arXiv:1610.03507.

[GS10] O. Gühne and M. Seevinck. Separability criteria for genuine multiparticle entanglement. *New Journal of Physics* 12(5):053002 (2010), arXiv:0905.1349.

[HBC24] S. Huang, K. R. Brown, and M. Cetina. Comparing Shor and Steane error correction using the Bacon-Shor code. *Science Advances* 10 (2024), arXiv:2312.10851.

[HDHL24] Y. Hong, E. Durso-Sabina, D. Hayes, and A. Lucas. Entangling four logical qubits beyond break-even in a nonlocal code. *Phys. Rev. Lett.* 133:180601 (2024), arXiv:2406.02666.

[HF19] R. Harper and S. T. Flammia. Fault-tolerant logical gates in the IBM Quantum Experience. *Phys. Rev. Lett.* 122:080504 (2019), arXiv:1806.02359.

[JP22] S. Jandura and G. Pupillo. Time-optimal two-and three-qubit gates for Rydberg atoms. *Quantum* 6:712 (2022), arXiv:2202.00903.

[KLR+22] S. Krinner, N. Lacroix, A. Remm, et al. Realizing repeated quantum error correction in a distance-three surface code. *Nature* 605:669–674 (2022), arXiv:2112.03708.

[Kni05] E. Knill. Quantum computing with realistically noisy devices. *Nature* 434:39 (2005), arXiv:quant-ph/0410199.

[Kre24] M. Krenn. Largest genuine entanglement: Qubits in GHZ state. `mariokrenn.wordpress.com/2021/01/29/reference-list-for-records-in-large-entanglement-generation-number-of-qubits-in-ghz-states` , 2024.

[LGL+17] N. M. Linke, M. Gutierrez, K. A. Landsman, et al. Fault-tolerant quantum error detection. *Science Advances* 3(10):1701074 (2017), arXiv:1611.06946.

[LGM+24] T. Lubinski, J. J. Goings, K. Mayer, et al. Quantum algorithm exploration using application-oriented performance benchmarks. (2024), arXiv:2402.08985.

[LJV+23] T. Lubinski, S. Johri, P. Varosy, et al. Application-oriented performance benchmarks for quantum computing. *IEEE Trans. Quantum Eng.* 4:1–32 (2023), arXiv:2110.03137.

[LMRM17] N. M. Linke, D. Maslov, M. Roetteler, and C. Monroe. Experimental comparison of two quantum computing architectures. *Proc. Natl. Acad. Sci.* 114(13):3305–3310 (2017), arXiv:1702.01852.

[MBA+23] S. A. Moses, C. H. Baldwin, M. S. Allman, et al. A race-track trapped-ion quantum processor. *Phys. Rev. X* 13:041052 (2023), arXiv:2305.03828.

[MLM+19] P. Murali, N. M. Linke, M. Martonosi, et al. Full-stack, real-system quantum computer studies: architectural comparisons and design insights. In *Proc. ISCA*, pages 527–540, 2019, arXiv:1905.11349.

[MLP+23] S. Ma, G. Liu, P. Peng, et al. High-fidelity gates and mid-circuit erasure conversion in an atomic qubit. *Nature* 622(7982):279–284 (2023), arXiv:2305.05493.

[NC+23] M. A. Norcia, W. B. Cairncross, et al. Midcircuit qubit measurement and rearrangement in a ^{171}Yb atomic array. *Phys. Rev. X* 13:041034 (2023), arXiv:2305.19119.

[NKC+24] M. Norcia, H. Kim, W. Cairncross, et al. Iterative assembly of ^{171}Yb atom arrays with cavity-enhanced optical lattices. *PRX Quantum* 5:030316 (2024), arXiv:2401.16177.

[PBP+24] L. Postler, F. Butt, I. Pogorelov, et al. Demonstration of fault-tolerant Steane quantum error correction. *PRX Quantum* 5:030326 (2024), arXiv:2312.09745.

[PL23] B. Pokharel and D. A. Lidar. Demonstration of algorithmic quantum speedup. *Phys. Rev. Lett.* 130:210602 (2023), arXiv:2207.07647.

[PNH+24] H. Putterman, K. Noh, C. T. Hann, et al. Hardware-efficient quantum error correction using concatenated bosonic qubits. (2024), arXiv:2409.13025.

[PSE96] G. M. Palma, K.-A. Suominen, and A. K. Ekert. Quantum computers and dissipation. *Proc. R. Soc. Lond. A* 452:567–584 (1996), arXiv:quant-ph/9702001.

[PSR+24] A. Paetznick, M. Silva, C. Ryan-Anderson, et al. Demonstration of logical qubits and repeated error correction with better-than-physical error rates. 2024, arXiv:2404.02280.

[RAC+24] B. W. Reichardt, D. Aasen, R. Chao, et al. Demonstration of quantum computation and error correction with a tesseract code. (2024), arXiv:2409.04628.

[RBL+21] C. Ryan-Anderson, J. G. Bohnet, K. Lee, et al. Realization of real-time fault-tolerant quantum error correction. *Phys. Rev. X* 11:041058 (2021), arXiv:2107.07505.

[RCC+24] A. G. Radnaev, W. C. Chung, D. C. Cole, et al. A universal neutral-atom quantum computer with individual optical addressing and non-destructive readout, arXiv:2408.08288.

[Rei20] B. W. Reichardt. Fault-tolerant quantum error correction for Steane's seven-qubit color code with few or no extra qubits. *Quantum Sci. Technol.* 6(1):015007 (2020), arXiv:1804.06995.

[RHK+20] T. Roy, S. Hazra, S. Kundu, et al. Programmable superconducting processor with native three-qubit gates. *Phys. Rev. Applied* 14:014072 (2020), arXiv:1809.00668.

[SBA24] C. N. Self, M. Benedetti, and D. Amaro. Protecting expressive circuits with a quantum error detection code. *Nat. Phys.* 20:219–224 (2024), arXiv:2211.06703.

[Sho96] P. W. Shor. Fault-tolerant quantum computation. In *Proc. 37th Symp. on Foundations of Computer Science (FOCS)*, page 96, 1996, arXiv:quant-ph/9605011.

[SST+23] P. Scholl, A. L. Shaw, R. B.-S. Tsai, et al. Erasure conversion in a high-fidelity Rydberg quantum simulator. *Nature* 622(7982):273–278 (2023), arXiv:2305.03406.

[Ste97] A. M. Steane. Active stabilization, quantum computation, and quantum state synthesis. *Phys. Rev. Lett.* 78(11):2252 (1997), arXiv:quant-ph/9611027.

[VGW96] L. Vaidman, L. Goldenberg, and S. Wiesner. Error prevention scheme with four particles. *Phys. Rev. A* 54:R1745 (1996), arXiv:quant-ph/9603031.

[Vui18] C. Vuillot. Is error detection helpful on IBM 5Q chips? *Quantum Information and Computation* 18(11 & 12) (2018), arXiv:1705.08957.

[WBD+19] K. Wright, K. M. Beck, S. Debnath, et al. Benchmarking an 11-qubit quantum computer. *Nat. Commun.* 10:5464 (2019), arXiv:1903.08181.

[WKPT22] Y. Wu, S. Kolkowitz, S. Puri, and J. D. Thompson. Erasure conversion for fault-tolerant quantum computing in alkaline earth Rydberg atom arrays. *Nature Commun.* 13(1):4657 (2022), arXiv:2201.03540.

[WWJ+18] D. Willsch, M. Willsch, F. Jin, et al. Testing quantum fault tolerance on small systems. *Physical Review A* 98(5) (2018), arXiv:1805.05227.

[XZZ+24] Q. Xu, H. Zhou, G. Zheng, et al. Fast and parallelizable logical computation with homological product codes. (2024), arXiv:2407.18490.

[YDKR24] K. Yamamoto, S. Duffield, Y. Kikuchi, and D. M. Ramo. Demonstrating Bayesian quantum phase estimation with quantum error detection. *Phys. Rev. Research* 6:013221 (2024), arXiv:2306.16608.

[ZLC00] X. Zhou, D. W. Leung, and I. L. Chuang. Methodology for quantum logic gate construction. *Phys. Rev. A* 62:052316 (2000), arXiv:quant-ph/0002039.